Available online at www.sciencedirect.com
SCIENCE DIRECT®
Geochimica et Cosmochimica Acta 70 (2006) 697–710
Geochimica
www.elsevier.com/locate/gca

Host rock compositional controls on zircon trace element signatures in metabasites from the Austroalpine basement

Bernhard Schulz [a,*], Reiner Klemd [b], Helene Brätz [b]

[a] Institut für Geologie und Mineralogie, Schloßgarten 5, D-91054 Erlangen, Germany
[b] Institut für Mineralogie und Kristallstrukturlehre, Am Hubland, D-97074 Würzburg, Germany

Received 3 February 2005; accepted in revised form 23 September 2005

Abstract

Zircon populations of Neoproterozoic and early Paleozoic age occur in metabasites of a high-pressure amphibolite-facies unit of the Austroalpine basement south of the Tauern Window. The host rocks for these zircons are eclogitic amphibolites of N-MORB-type character, hornblende gneisses with volcanic-arc basalt signature, and alkaline within-plate-basalt amphibolites. Bulk rock magmatic trace element patterns were preserved during amphibolite-facies high-pressure and subsequent high-temperature events, as well as a greenschist-facies overprint. Positive Ce and negative Eu anomalies and enrichment of HREE in normalized zircon REE patterns, as analysed by LA-ICP-MS, are typical for an igneous origin of these zircon suites. Zircon Y is well correlated to HREE, Ce, Th, U, Nb, and Ta and allows discrimination of compositional fields for each host rock type. Low Th/U ratios are correlated to low Y and HREE abundances in zircon from low bulk Th/U host rocks. This is likely a primary igneous characteristic that cannot be attributed to metamorphic recrystallization. Variations of zircon/host rock element ratios confirm that ionic radii and charges control abundances of many trace elements in zircon. The trace element ratios—presented as mineral/melt distribution coefficients—indicate a selectively inhibited substitution of Zr and Si by HREE and Y in zircon which crystallized from a N-MORB melt. Correlated host rock and zircon trace element concentrations indicate that the metabasite zircons are not xenocrysts but crystallized from mafic melts, represented by the actual host rocks.

1. Introduction

Zircon plays a major role in U–Th–Pb radiometric dating of igneous crystallization and medium- to high-grade metamorphic processes. The significance of variable zircon populations and heterogeneous growth zones in igneous and high-grade metamorphic rocks is one of the main problems of U–Th–Pb chronology (Möller et al., 2002; Hoskin and Schaltegger, 2003) and can be addressed by trace element studies within zircon populations. Igneous and metamorphic zircon can be distinguished by their Th/U ratios and by Y, Nb, and HREE contents (Hoskin and Black, 2000; Rubatto, 2002; Hoskin and Schaltegger, 2003, and references therein). Trace elements in zircon are potential indicators of the igneous sources of kimberlites, carbonatites, and lamproites (Heaman et al., 1990; Hoskin and Ireland, 2000; Belousova et al., 2002). However, other workers reported the absence of significant trace element chemical differences between zircon populations derived from crustal rock types (Murali et al., 1983; Rupasinghe and Dissanayake, 1987; Snyder et al., 1993; Shannon et al., 1997; Chesner, 1998; Hoskin and Schaltegger, 2003). The question whether trace element compositions of zircon can be related to source rock characteristics is critical in provenance studies of detrital zircon in sedimentary rocks (e.g., Bodet and Schärer, 2000; Hoskin and Ireland, 2000; Wilde et al., 2001). Delineation and recognition of relationships between zircon compositions and source rock types are hampered by the limited availability of data from mafic rocks. The present study contributes trace element data determined by LA-ICP-MS on zircon extracted from high-pressure amphibolite-facies metabasites of Neoproterozoic and Early Paleozoic protolith ages.

* Corresponding author. Fax: +49 9131 852 9295.
E-mail address: bschulz@geol.uni-erlangen.de (B. Schulz).

0016-7037/$ - see front matter © 2005 Elsevier Inc. All rights reserved.
doi:10.1016/j.gca.2005.10.001

2. Geological setting

The Austroalpine basement south of the Tauern Window (Fig. 1A) is one of the pre-Early Ordovician units in the Alps (Von Raumer and Neubauer, 1993; Schulz et al., 1993; Von Raumer et al., 2003). A pre-Alpine (Carboniferous/Permian) high-pressure amphibolite-facies metamorphic event with crystallization of garnet, staurolite and kyanite in metapelites, as well as garnet and omphacite in metabasites, can be recognized at least in some parts (Schulz, 1990, 1993, 1997). Early- and Late-Alpine deformation and metamorphism overprinted the pre-Alpine structures and mineral assemblages to variable degrees (Hoinkes et al., 1999).

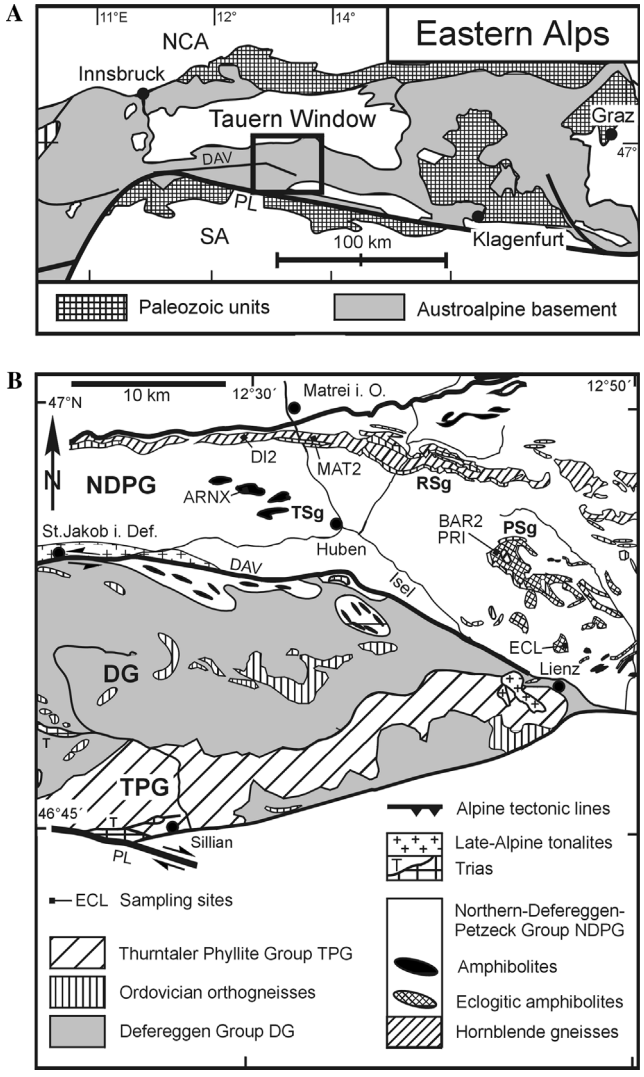

Fig. 1. (A) Tectonic units in the Eastern Alps. (B) Lithological units in the Austroalpine basement to the south of the central Tauern Window, Eastern Alps, with sampling locations for the zircon-bearing metabasites investigated in this study. DAV, Defereggen-Antholz-Vals line; DG, Defereggen Group; NDPG, Northern-Defereggen-Petzeck Group; P, Penninic unit; PL, Periadriatic Lineament; PSg, Prijakt Subgroup (eclogitic amphibolites and hornblende gneisses); RSg, Rotenkogel Subgroup (hornblende gneisses); TPG, Thurntaler Phyllite Group; TSg, Torkogel Subgroup (amphibolites).

In the meta-psammopelitic sequences of the Northern-Defereggen-Petzeck Group (Fig. 1B) metabasites occur in layers of several 100 m thickness and in numerous isolated meter-scale lenses. Whole-rock element variations in the metabasites can be attributed to magmatic fractionation and allow us to distinguish rock suites (Schulz et al., 1993; Schulz, 1995, 1997; Schönhofer, 1999). Zircon-bearing samples that are characteristic for a N-MORB suite of eclogitic amphibolites are specimens PRI and BAR2 from the Barrenle See location (E 12°42′35″/N 46°54′52″), and ECL collected along the road from Lienz-Oberdorf to Zettersfeld (E 12°46′28″/N 46°51′24″) in the Schobergruppe. Samples DI2 (E 12°30′05″/N 46°58′56″) and MAT2 (E 12°33′30″/N 46°58′50″) from a volcanic-arc basalt (VAB) suite are hornblende gneisses obtained along forest roads to the NW of Arnitzalm and to the south of Matrei at Außer Klaunzer Berg, respectively. A within-plate-basalt (WPB) suite is represented by the garnet amphibolite sample ARNX (E 12°30′03″/N 46°56′45″) from Arnitzalm (Fig. 1B).

3. Analytical methods

The whole-rock compositions of the metabasites (Table 1) were obtained by LA-ICP-MS analysis at the Institut für Mineralogie und Kristallstrukturlehre, University of Würzburg with a single collector quadrupole AGILENT 7500i ICP-MS equipped with a 266 nm Merchantek LUV 266x laser. Argon was used as the carrier gas. The laser was adjusted to a scan speed of 5 μm/s at an energy of 0.25 mJ and a repetition rate of 10 Hz. It was traced along 1.6 mm long and 50 μm wide extraction lines on $LiBO_4$ fusion glass beads (Brätz and Klemd, 2002). Bulk rock concentrations of SiO_2 measured by XRF were used for normalization of LA-ICP-MS analyses. The glass reference material NIST SRM 612 with the values of Pearce et al. (1997) was used for external calibration and calculation of trace elements by the GLITTER Version 3.0 On-line Interactive Data Reduction for LA-ICP-MS Program of the year 2000 by Macquarie Research Ltd. Mean results from 5 extraction lines coincide within 1σ error with the data from acid solution ICP-MS (CRPG-CNRS Nancy, Schulz et al., 2004), except for the results for the element La. A constant amount of ~7 ppm La was introduced with $LiBO_4$ into the glass beads and was empirically corrected by regression through comparison of samples with different La concentrations (Sylvester, 2003). Based on the means calculated from 5 extraction lines, the error is <5% (based on 1σ standard deviation) for the REE, Hf, Nb, and Ta, except for Sm, Lu, Hf, and Th (5 to 13%) in sample ECL. Reproducibility, accuracy and precision of the applied method were controlled by repeated analysis of NIST SRM 614 (SIMS data by Horn et al., 1997) and whole-rock geostandards (BE-N Basalt, MAG-1 Marine Mud; Govindaraju, 1994). Based on analysis of NIST SRM 614, the precision for REE, Nb, Ta, and Th is <5% (based on 1σ), except for Gd and Er (5–7.5%).

Table 1
Whole-rock major and trace element data (LA-ICP-MS) of zircon-bearing Austroalpine metabasites

Sample	ECL ecl-am N-MORB	MAT2 hbl-gn VAB	DI2 hbl-gn VAB	ARNX am WPB
SiO_2 (wt.%)	48.30	53.50	60.10	50.50
TiO_2	1.48	0.39	0.61	2.76
Al_2O_3	17.90	17.87	16.45	17.20
Fe_2O_3	9.11	5.96	6.52	9.58
MnO	0.13	0.10	0.10	0.12
MgO	6.43	6.57	3.22	3.34
CaO	11.39	9.32	6.19	7.56
Na_2O	3.63	2.66	3.45	5.17
K_2O	0.41	0.58	0.91	0.82
P_2O_5	0.09	0.06	0.10	0.69
LOI	0.99	2.26	1.76	1.92
Total	99.85	99.27	99.42	99.67
Cr (ppm)	358	58	45	61
V	266	114	145	165
Co	43	31	18	26
Ni	67	75	31	18
Zn	85	43	77	91
Ga	19	16	18	26
Rb	8	11	19	24
Sr	185	348	296	310
Y	21	7	19	31
Zr	88	45	124	389
Nb	1.7	1.7	4.3	59.8
Ba	106	156	332	314
La	1.71	5.15	9.66	39.96
Ce	8.93	12.22	25.02	92.25
Pr	1.45	1.47	3.38	10.65
Nd	7.94	6.02	15.02	42.70
Sm	2.47	1.42	3.36	8.77
Eu	1.15	0.52	0.89	2.71
Gd	3.23	1.29	3.23	7.56
Tb	0.55	0.21	0.50	1.09
Dy	3.89	1.27	3.43	6.42
Ho	0.79	0.26	0.70	1.18
Er	2.29	0.73	2.07	3.30
Tm	0.35	0.11	0.34	0.48
Yb	2.44	0.84	2.33	3.22
Lu	0.33	0.12	0.35	0.43
Hf	1.59	1.36	3.25	6.73
Ta	0.17	0.13	0.30	3.40
Pb	1.69	2.53	5.11	5.63
Th	0.09	1.33	2.57	5.88
U	0.51	0.60	1.75	1.88
$\delta^{18}O_{SMOW}{}^{*}$	8.0		7.1	9.3
$^{143}Nd/^{144}Nd_{INIT}{}^{*}$	0.512229	0.511946	0.511813	0.512195
$^{87}Sr/^{86}Sr_{INIT}{}^{*}$	0.70333	0.70369	0.70405	0.70520
Age (Ma)*	590 ± 4	548 ± 4	543 ± 2	430 ± 2
$(La/Yb)_N$	0.35	4.15	2.81	8.39
Th/U	0.18	2.19	1.46	3.14

Isotope initials marked by stars refer to protolith ages and data in Schulz et al. (2004) and are given for evaluation of magmatic sources. Rock types are eclogitic amphibolite (ecl-am), hornblende gneiss (hbl-gn), amphibolite (am), and their geochemical characteristics refer to mid ocean ridge basalt (N-MORB), volcanic-arc basalt (VAB), within-plate basalt (WPB).

Zircon grains 125–100 μm in size were separated using standard magnetic and heavy liquid separation techniques. Transparent and slightly coloured crystals were embedded and polished. Imaging by electron microscopy (REM) and cathodoluminescence (CL) revealed homogeneous crystals with no distinct cores. One part of the grain populations was used for Pb–Pb single zircon evaporation dating (Schulz and Bombach, 2003). Trace elements in about 80 zircon grains from 6 metabasite samples were analysed with LA-ICP-MS. The laser was traced along 100 μm long and 30 μm wide lines and adjusted to a scan speed of 5 μm/s at an energy of 0.25 mJ and a repetition rate of 10 Hz.

Time resolved signals for Sr, REE, Y, Zr, Hf, Nb, Ta, Th, and U were compared to those from glass reference material NIST 612 and 614 (Jackson et al., 1992; Norman et al., 1996; Pearce et al., 1997). SiO_2 (33 wt.%) was used as internal standard. Signals for P in zircon cannot be distinguished from background. After signal quantification by the GLITTER Version 3.0 On-line Interactive Data Reduction for LA-ICP-MS Program of the year 2000 by Macquarie Research Ltd, the 1σ error based on counting statistics from signal and background ranges between 27% for Ta (0.77 ± 0.20 ppm) and 4% for Yb (309 ± 13.8 ppm), depending on absolute concentrations. Reproducibility, accuracy, and precision were controlled by repeated analysis of NIST SRM 614.

4. Zircon host rock characteristics

Variations in whole-rock Zr and Ti inter-element characteristics of the metabasite layers in larger outcrops (Fig. 1B) allowed us to distinguish basaltic rock suites, following the method of Pearce (1982). Intra-suite element variations can be attributed to magmatic fractionation, as exemplified in a Zr–Y plot (Fig. 2A) leading to zircon-bearing fractionates (Table 1). Further characterization of the suites was possible on the basis of rare earth and trace element data (Schulz, 1995; Schulz and Bombach, 2003; Schulz et al., 2004), and is discussed in the following sections.

4.1. N-MORB-type suite

Eclogitic amphibolites such as sample ECL (Fig. 1B) have a high-pressure mineral assemblage with pyrope- and grossular-rich garnet, omphacite (Jd_{42}), plagioclase (An_7), rutile, and quartz that crystallized at 14–16 kbar and 550–650 °C. A subsequent amphibolite-facies assemblage with pargasite indicates metamorphic conditions at 680 °C and 10 kbar (Schulz, 1993). The Zr–Ti abundances correspond to N-MORB (Schulz et al., 1993), however, large ion lithophile (LIL) elements and Ce in the suite are slightly enriched in comparison to MORB (Schulz, 1995). Chondrite normalized (normalization values from McDonough and Sun, 1995) REE patterns reflect slight LREE enrichment (Fig. 2B) and low fractionation ($[La/Yb]_N$ 0.3–1.8). Trace element and whole-rock isotope characteristics were interpreted to indicate back arc magmatism (Schulz et al., 2004). Layered dikes or sills could have been the magmatic protoliths of the Prijakt eclogitic amphibolites as can be concluded from their appearance in the field, the lithological layering, and the intra-suite element variations (Schulz, 1995).

4.2. Volcanic-arc-basalt-type suite

Hornblende gneisses appear in dm-to-m thick layers with flaser structure. Ca-amphibole of an amphibolite-facies mineral assemblage occurs in up to 0.5 cm lens-like

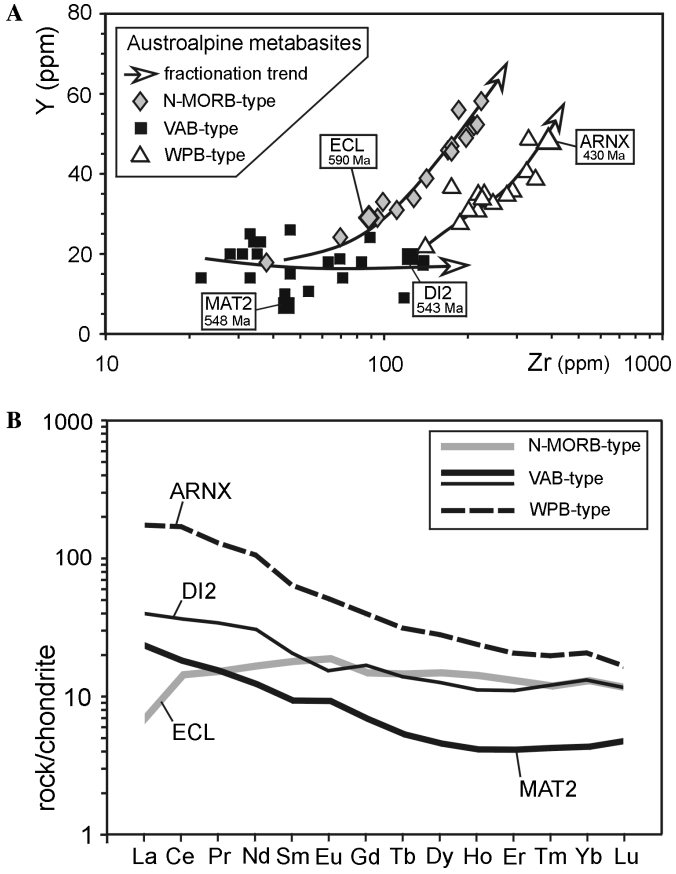

Fig. 2. (A) Austroalpine metabasite suites with zircon-bearing fractionates in the Zr–Y plane. Samples dated by Pb–Pb single zircon evaporation and used for zircon trace element study are labelled. Intra-suite magmatic fractional crystallization trends are indicated by arrows. (B) Whole-rock REE patterns of Austroalpine metabasite suites, normalized to chondrite (normalization factors after McDonough and Sun, 1995). N-MORB-type suite: eclogitic amphibolites, Prijakt Subgroup. Volcanic-arc basalt (VAB-type) suite: hornblende gneisses, Rotenkogel Subgroup. Within-plate-basalt (WPB-type) suite: amphibolites, Torkogel Subgroup. Data compiled from Schulz (1995), Schulz and Bombach (2003), Schulz et al. (2004), and this study.

aggregates which are surrounded by a foliated matrix composed of plagioclase, epidote, and quartz. Retrogressive replacement of amphibole by chlorite and epidote of an Alpine greenschist-facies overprint is frequently observed. Bulk rock Zr and Ti abundances correspond to volcanic-arc-basalt (VAB). The hornblende gneisses follow a calc-alkaline fractionation trend with Zr/Y from 1.3 to 13.1 (Fig. 2A). They show enrichment of Sr, K_2O, Rb, Ba, Th, and Ce relative to MORB. Tantalum, Nb, Zr, Hf, Sm, Ti, Y, Yb, and Cr are relatively depleted when compared to MORB (Schulz, 1997; Schönhofer, 1999; Schulz and Bombach, 2003; Schulz et al., 2004). Both features are characteristics of magma generated in island arc and active continental margin settings (Wilson, 1989). LREE are elevated over HREE (Fig. 2b) and $(La/Yb)_N$ ratios range from 2 to 8. Major element characteristics and the presence of hornblendites interpreted as former autoliths support a plutonic origin for these hornblende gneisses (Schulz et al., 2004).

4.3. Within-plate-basalt-type suite

Amphibolites with Ca-amphibole, plagioclase, garnet, sphene, epidote, chlorite, and quartz show no relicts of former eclogite-facies metamorphism. They have transitional to alkaline compositions and display elevated Zr and Ti contents corresponding to within-plate-basalts (WPB). The Nb (39.6–58.8 ppm) and Ta (3.4–8.2 ppm) contents are significantly higher than those of the N-MORB- and VAB-type rocks. There is considerable enrichment in LILE and HFSE, and the REE are strongly fractionated (Fig. 2B), with $(La/Yb)_N$ ratios between 8 and 13. A large range of initial $^{87}Sr/^{86}Sr$ characteristic of this suite is interpreted to result from a variable contribution of enriched mantle and/or continental crust to a main depleted mantle source (Schulz et al., 2004). Among these mafic suites, the geochemical signatures of source contamination by a crustal magma are most developed in the WPB-type rocks. Dikes or sills are considered to be the magmatic protoliths of the amphibolites, as can be concluded from their widely distributed appearance in the field (Schulz et al., 1993).

5. Zircon morphology and ages

A uniform population of clear, short prismatic to round zircon from N-MORB-type sample ECL displays intense blue CL colours and is characterized by intact crystal lattices. The crystals are homogeneous without xenocrystic cores and inclusions. No distinct rims and domains, attributed to a late- to post-magmatic or metamorphic recrystallization, as described by Corfu et al. (2003), have been observed. This zircon has low $^{204}Pb/^{206}Pb$ and uniform Pb–Pb evaporation ages of around 590 ± 4 Ma (Schulz and Bombach, 2003). In contrast to observations from sample ECL, zircon in the N-MORB-type samples PRI and BAR2 is whitish and prismatic, with etched crystal faces. The CL images indicate crystal defects by yellow colours and extinguished oscillatory zonation. Accordingly, $^{204}Pb/^{206}Pb$ in the zircon is elevated. Zircon ages display a large scatter from 412 ± 7 to 338 ± 13 Ma and are considered to have been arbitrarily reset during Variscan and Alpine metamorphism (Schulz and Bombach, 2003).

In zircon from the VAB-type hornblende gneisses the symmetry of oscillatory growth zoning and sector zoning is not always related to the crystal faces. Distinct xenocrystic cores have not been detected. Some crystals have small inclusions, probably apatite. Zircon displays low $^{204}Pb/^{206}Pb$ ratios and gave uniform Pb–Pb evaporation ages of 543 ± 2 Ma (DI2) and 548 ± 4 Ma (MAT2, Schulz and Bombach, 2003).

The alkaline WPB-type garnet-amphibolite sample ARNX, with a high-bulk rock Zr concentration (Fig. 2A), was selected for the study, as zircon can be expected to crystallize from a Zr-rich differentiate. The sample contains a uniform population of whitish or clear zircon that does not have xenocrystic cores. Crystal faces are sutured and pitted, a morphological feature which can be attributed to partial resorption of grains in a magma (Corfu et al., 2003). Pb–Pb evaporation data from zircon in this sample yielded uniform ages averaged at 430 ± 2 Ma (Schulz and Bombach, 2003).

The internal oscillatory and sector zoning in zircon from samples ECL, DI2, MAT2, and ARNX are features which can be attributed to growth in a melt (Hanchar and Miller, 1993; Vavra, 1994; Connelly, 2000). However, this feature was also observed in high-pressure metamorphic zircon (Corfu et al., 2003), and further criteria for a distinction are necessary.

6. Zircon REE pattern

The REE contents in zircon (Table 2) were normalized to chondrite values after McDonough and Sun (1995). Zircon from the N-MORB-type garnet-bearing eclogitic amphibolite sample ECL has low concentrations of LREE with depletion of La compared to C1. The HREE display an increasing enrichment (Gd 10 times, Lu 1000 times C1) with decreasing ionic radii (Fig. 3A). Positive Ce and negative Eu anomalies, typical of terrestrial igneous zircon (Hoskin and Schaltegger, 2003), are observed. This pattern is matched by most of the zircon grains from the VAB-type samples DI2 and MAT2 and the WPB-type metabasite sample ARNX (Figs. 3B and C).

In contrast, some zircon grains from the VAB-type host rock sample DI2 display significantly elevated LREE with a similar degree of enrichment of La over Sm (100 times C1), no positive Ce anomaly, and a poorly developed negative Eu anomaly (Table 3, Fig. 3B). Such a pattern was observed by Jain et al. (2001) in bulk zircon analyses and attributed to the presence of mineral inclusions (Hoskin and Schaltegger, 2003). In situ analyses with this pattern could be explained by the possible presence of small or submicroscopic apatite inclusions. Furthermore, corroded zircon with elevated common Pb (Schulz and Bombach, 2003) from PRI and BAR2 has highly variable La and Ce contents, and a positive Ce anomaly is not developed. Incoherent and scattered HREE patterns with highly variable enrichment over HREE prevail, and Lu is low in some of the altered zircon grains (Fig. 3D).

Similar REE patterns are observed from the zircon grains with no signs of alteration. When mean values calculated from three characteristic and complete zircon analyses from each sample and the overall pattern from each suite are compared (Table 2, Fig. 3E), concentrations of REE and especially the LREE are higher in the WPB than in the N-MORB- and VAB-type samples (Fig. 3E). Furthermore, zircon HREE in the WPB-type sample are less fractionated than in the other samples. In detail, the $(Yb/Dy)_N$ ratio ranges in WPB-type zircon from 4.1 to 5.8, in VAB-type zircon from 5.8 to 12.5 and in N-MORB-type zircon from 12.5 to 25 (Fig. 3E). The Eu/Eu* are slightly variable and never exceed 0.5.

Table 2
Representative trace element analyses of zircon (LA-ICP-MS) from eclogitic amphibolite (ecl-am), hornblende gneiss (hbl-gn), and amphibolite (am)

Sample	ECL				MAT2				DI2				ARNX			
	e9-8c ecl-am N-MORB	9a-8g ecl-am N-MORB	9a-8b ecl-am N-MORB	mean N-MORB	f1-4d hbl-gn VAB	7a-9a hbl-gn VAB	f1-4b hbl-gn VAB	mean VAB	f1-8e hbl-gn VAB	f1-7c hbl-gn VAB	f1-1e hbl-gn VAB	mean VAB	d7-4e am WPB	7a-4a am WPB	d7-4b am WPB	mean WPB
Sr	0.77	0.37	0.36	0.50	0.58	1.63	0.91	1.04	1.97	2.94	2.23	2.38	1.25	0.60	0.58	0.81
Y	171	193	186	183	457	1288	683	809	819	822	826	822	1398	1955	1861	1738
Nb	0.43	0.66	1.06	0.72	2.13	2.78	1.19	2.03	1.34	0.70	0.87	0.97	27.50	10.90	17.60	18.67
La	0.22	0.17	0.04	0.15	0.04	0.59	0.31	0.31	0.28	0.11	1.40	0.59	1.14	0.45	1.12	0.90
Ce	1.91	0.89	1.14	1.31	3.32	12.80	3.50	6.54	4.27	5.13	7.35	5.58	41.90	20.20	12.70	24.93
Pr	0.07	0.07	0.07	0.07	0.01	0.41	0.32	0.25	0.10	0.15	0.08	0.11	0.61	0.41	0.40	0.47
Nd	0.40	0.78	0.77	0.65	0.39	1.67	2.42	1.49	4.19	1.16	0.38	1.91	4.90	4.85	4.00	4.58
Sm	3.20	0.88	1.13	1.74	6.88	1.22	3.14	3.75	3.96	2.97	1.81	2.91	9.70	8.52	7.00	8.41
Eu	0.36	0.07	0.03	0.15	0.74	0.15	0.67	0.52	1.17	0.17	0.78	0.70	1.00	1.64	1.47	1.37
Gd	3.42	2.39	3.21	3.01	9.11	13.10	9.14	10.45	14.20	18.15	12.58	14.97	31.30	44.10	34.90	36.77
Tb	1.09	0.42	0.77	0.76	1.86	6.42	3.65	3.98	3.37	5.47	3.25	4.03	15.20	15.60	13.90	14.90
Dy	9.49	11.20	11.20	10.63	29.10	78.30	36.10	47.83	52.4	63.60	53.84	56.61	178.00	194.00	148.60	173.53
Ho	5.89	5.03	5.11	5.34	13.40	36.70	17.70	22.60	22.08	25.07	22.16	23.10	56.90	70.60	45.40	57.63
Er	30.38	27.10	30.80	29.43	56.40	175.00	77.50	102.97	107.00	136.70	122.30	122.00	246.00	315.00	274.40	278.47
Tm	8.02	7.07	6.57	7.22	16.20	46.10	23.50	28.60	21.91	30.60	26.00	26.17	52.30	72.10	57.60	60.67
Yb	114	105	84	101	225	567	218	337	220	289	266	258	499	630	441	523
Lu	27	22	21	24	49	125	52	75	64	60	54	59	83	103	101	96
Hf	11303	7902	7782	8996	8462	11710	4450	8207	11445	8749	8228	9474	9938	5203	6525	7222
Ta	1.15	0.41	0.49	0.68	0.34	1.71	0.65	0.90	0.91	0.33	0.50	0.58	6.80	3.98	5.50	5.43
Th	3.73	3.13	2.45	3.13	65.54	294	232	197	32.80	35.12	24.88	30.93	301	596	169	355
U	116	94	73	94	122	426	249	266	217	126	123	155	337	367	136	280
Th/U	0.03	0.03	0.03	0.12	0.54	0.69	0.93	0.74	0.15	0.28	0.20	0.21	0.89	1.62	1.24	1.27
$(Yb/Dy)_N$	18.27	14.32	11.49	14.50	11.81	11.06	9.22	10.75	6.44	6.95	7.55	6.98	4.28	4.96	4.53	4.61
Eu/Eu*	0.33	0.15	0.04	0.20	0.28	0.11	0.38	0.25	0.47	0.07	0.50	0.34	0.17	0.26	0.29	0.24

Selection of data is based on analyses which cover the complete list of elements above detection limit and main focus of compositional fields in Fig. 4. Geochemical characteristics of zircon host rocks are mid ocean ridge basalt (N-MORB), volcanic-arc basalt (VAB), and within-plate basalt (WPB). Normalized to C1 of McDonough and Sun (1995), calculation of $Eu/Eu^* = Eu/\sqrt{(La * Pr)}$ from the normalized values (Hoskin and Schaltegger, 2003).

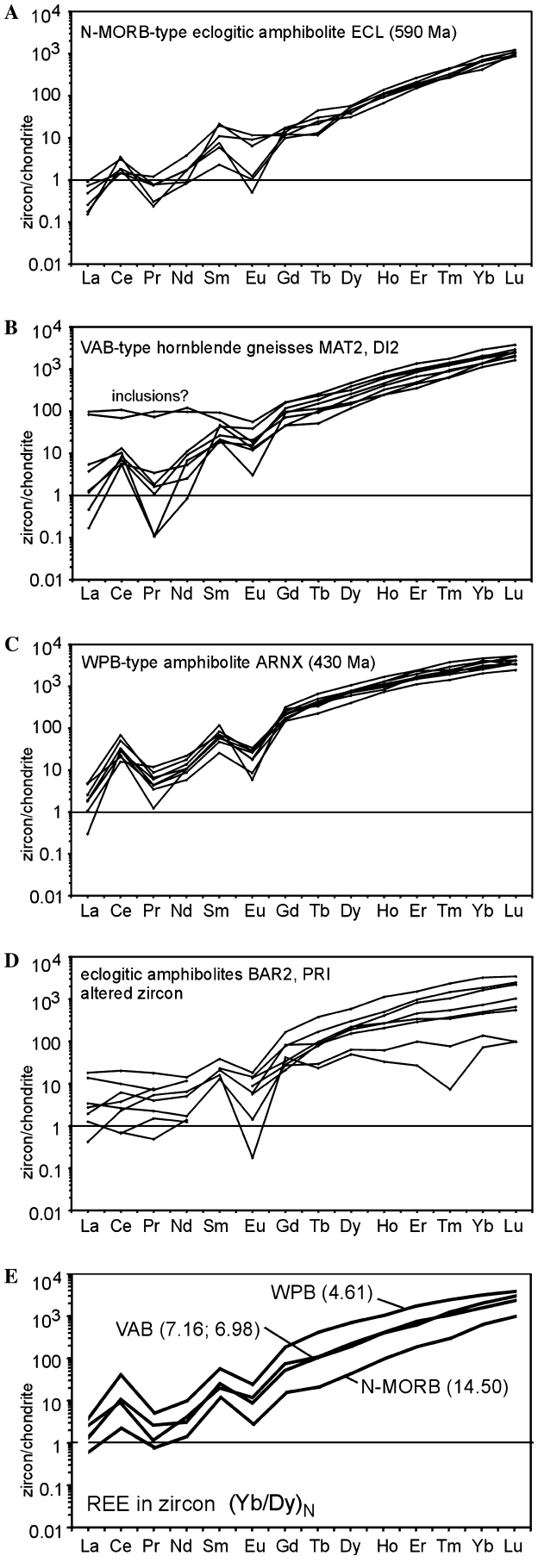

Table 3
Trace element analyses (LA-ICP-MS) of zircon with submicroscopic inclusions from hornblende gneiss (hbl-gn) and zircon with postmagmatic alteration from eclogitic amphibolite (ecl-am)

Sample	DI2		BAR2	PRI
	f1-1b	f1-1h	e9-9c	g4-8b
	hbl-gn	hbl-gn	ecl-am	ecl-am
	VAB	VAB	N-MORB	N-MORB
Sr	12.95	51.90	9.20	3.40
Y	568	954	1877	57
Nb	1.27	1.22	2.37	0.39
La	23.08	19.80	4.30	0.10
Ce	66.10	42.20	12.38	1.40
Pr	6.75	9.13	1.66	0.50
Nd	55.20	44.10	6.41	2.96
Sm	9.06	13.70	5.69	2.36
Eu	1.03	3.15	1.02	0.01
Gd	19.39	32.80	33.06	8.35
Tb	4.14	8.38	13.64	0.84
Dy	39.30	78.40	145.10	12.20
Ho	13.50	32.90	61.50	1.80
Er	72.70	145.50	243.00	4.30
Tm	15.50	32.40	58.00	0.18
Yb	179.90	333.00	520.00	11.60
Lu	39.90	60.40	84.50	2.40
Hf	6375	7110	11550	10479
Ta	2.51	2.32	1.85	2.33
Th	29	302	40	1.75
U	118	337	108	62
Th/U	0.25	0.90	0.37	0.03
$(Yb/Dy)_N$	7.00	6.49	5.48	1.45
Eu/Eu*	0.24	0.45	0.23	0.01

Normalized to C1 of McDonough and Sun (1995), calculation of $Eu/Eu^* = Eu/\sqrt{(La * Pr)}$ from the normalized values (Hoskin and Schaltegger, 2003).

7. Zircon trace element compositional fields

According to the different degree of HREE enrichment and fractionation, the metabasite zircon populations cover distinct trace element compositional fields (Fig. 4). The chondrite-normalized HREE (Fig. 3E), as well as the Y contents in zircon display a systematic variation between the metabasite types. Zircon Y contents are low (100–300 ppm) in N-MORB-, intermediate (200–1600 ppm) in VAB- and elevated (1000–3000 ppm) in WPB-type samples (Figs. 4A, B, F, and G). This is within the ranges reported from zircon in basalts; the majority of zircon from granitoids has higher Y contents that exceed 3000 ppm (Belousova et al., 2002).

Fig. 3. Zircon REE pattern, normalized to chondrite (normalization factors after McDonough and Sun, 1995). (A) N-MORB-type eclogitic amphibolite with homogeneous $^{207}Pb/^{206}Pb$ single zircon evaporation ages. (B) VAB-type hornblende gneisses; flat LREE patterns may be caused by unintentional analysis of small inclusions. (C) WPB-type amphibolite. (D) Eclogitic amphibolites with variable $^{207}Pb/^{206}Pb$ single zircon evaporation ages and altered zircon. (E) General REE pattern and HREE fractionation $(Yb/Dy)_N$ of zircon from N-MORB-, VAB-, and WPB-type metabasite host rocks. Mean values calculated from selected and complete analyses in Table 2 and in Fig. 4.

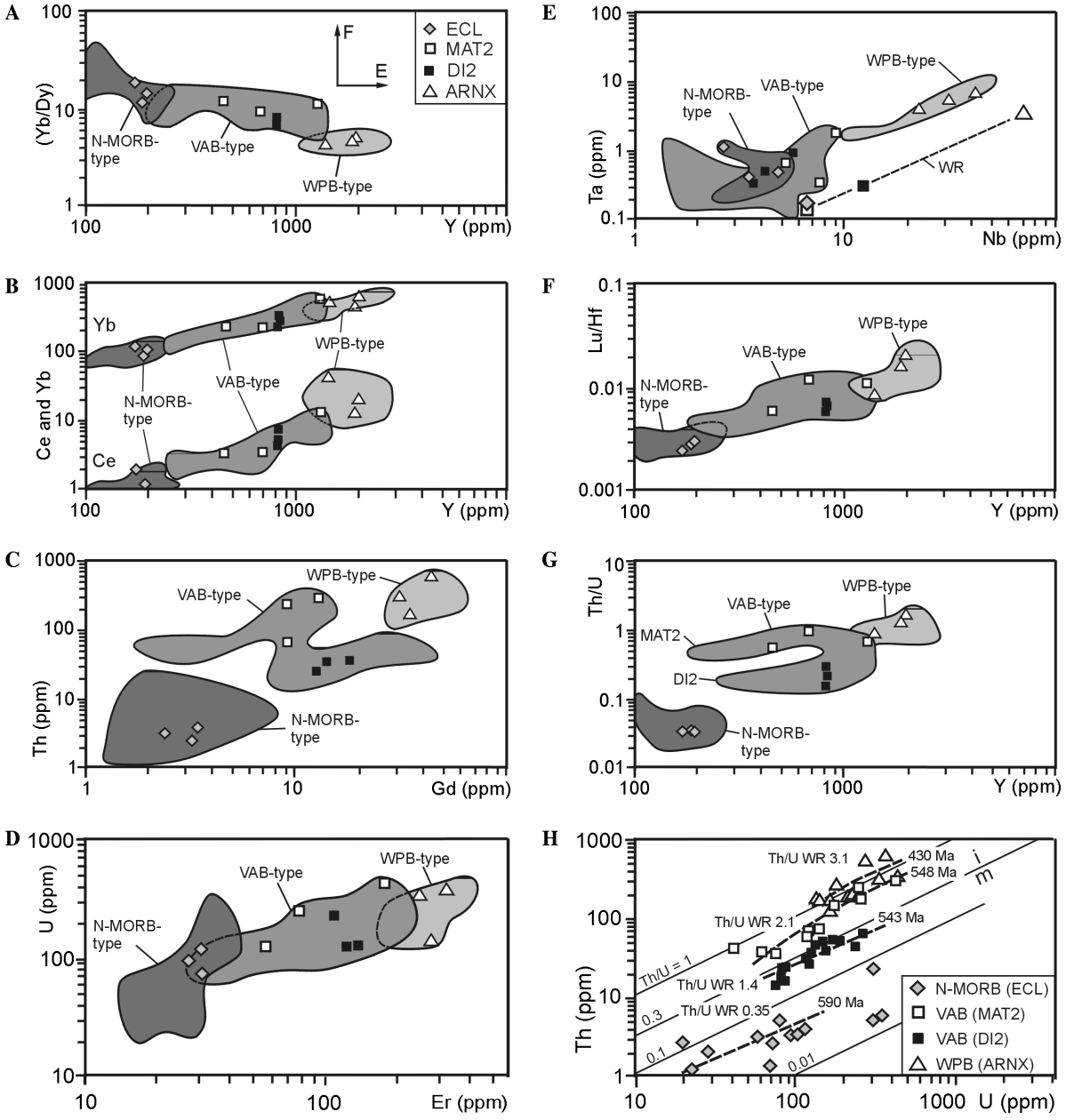

Fig. 4. Zircon trace element compositional fields, representing all available data; marked analyses are complete elemental analyses selected for calculation of mean values in Table 2; labels refer to rock suites in Figs. 2 and 5, normalized to chondrite (normalization factors after McDonough and Sun, 1995). (A) Y vs $(Yb/Dy)_N$ with vectors of HREE enrichment (E) and fractionation (F). (B) Y vs Ce and Yb. (C) Gd vs Th for demonstration of correlation between cations with similar ionic radius. (D) Er vs U for demonstration of correlation between cations with similar radius. (E) Correlation of Nb^{5+} vs Ta^{5+} and dependence on bulk rock abundances. (F) Correlation of zircon Y vs Lu/Hf due to invariable Hf; compare to Y vs Yb in (B). (G) Zircon Y vs Th/U with distinct Th-rich zircon in sample MAT2. (H) Zircon U vs Th and Th/U_{WR} (whole-rock) of zircon host rocks. Note subparallel regression (broken lines) at constant Th/U for each zircon population and dependence of zircon Th/U on host rock Th/U_{WR}. Line Th/U = 0.3 marks lower limit for igneous zircon (I) compared to metamorphic zircon (M) as proposed by Schaltegger et al. (1999).

The trend of decreasing HREE fractionation with increasing concentration (Fig. 3E) is confirmed in the zircon $(Yb/Dy)_N$ vs Y abundance diagram (Fig. 4A). Zircon Yb and Ce as well as Th and U (not shown) increase with increasing Y contents (Fig. 4B). The Th^{4+} (ionic radius 1.05 Å, Shannon, 1976) abundance increases and is correlated with $^{[8]}Gd^{3+}$ abundances (Fig. 4C). This element has a similar ionic radius (1.050 Å) and concentration in zircon. Similarly, U^{4+} (IR 1.00 Å) contents are correlated with the $^{[8]}Er^{3+}$ abundances. Erbium has an ionic radius of 1.004 Å (Fig. 4D).

Concentrations of Nb and Ta are low in zircon from N-MORB- and VAB-type host rocks, when compared to those of zircon from the WPB-type host rock, and reflect the respective host rock bulk concentrations. Although Nb and Ta are correlated in zircon, the fields of N-MORB- and VAB-type overlap (Fig. 4E) and can only be distinguished by using elements such as Y. In zircon, Nb concen-

trations are higher than those of Ta, although ionic radii and charge are equivalent. This appears to be a consequence of the bulk rock concentrations, where Nb contents exceed those of Ta by about one order of magnitude. Zircon Lu is similarly correlated with Y and Yb (Figs. 4B and F), but Hf does not reveal any co-variation with Y. Hf abundance in zircon does not exceed 12,000 ppm (Fig. 4F), which is in general agreement with observations from other mafic rocks (Belousova et al., 2002).

A subdivision of the zircon compositional fields is evident in the Y vs Th/U and Gd vs Th relationships for the VAB-type host rocks (Figs. 4C and G). Zircon in N-MORB-type sample ECL has low Th (1–8 ppm) and U values (20–100 ppm), and Th/U ratios scatter around 0.03. Zircon in the VAB-type hornblende gneisses has intermediate Th (10–200 ppm) and U (60–400 ppm) concentrations with Th/U ratios ranging from 0.2 to 1. The WPB-type amphibolite has zircon with comparatively elevated Th (100–600 ppm) and U (200–400 ppm) contents, at Th/U ratios around 1 (Fig. 4H). A dependence of zircon Th/U on the bulk rock Th/U ratio is evident (Fig. 4H).

8. Zircon and host rock trace element correlations

As the metabasite zircon populations display distinct trace element compositions, it must be evaluated whether they are related to the geochemical characteristics of the bulk host rocks (Fig. 4, Table 1). Mean values of trace element abundances in the respective zircon populations have been plotted against the corresponding whole-rock data (Fig. 5). Zircon Nb and Ta directly reflect the whole-rock abundances, and a similar correlation is observed for Th, but not for Sr and Hf. Abundances of Hf are almost similar in all zircon populations. Zircon vs whole-rock Y abundances show the same behavior as the HREE with even atomic number (Figs. 5A and B). For the VAB- and WPB-type samples, HREE with an atomic number >157 (Gd) display systematic and log–log linear positive correlations (Fig. 5B). Furthermore, the positions of the connection lines in the whole-rock vs zircon element abundances diagram (Fig. 5B) clearly reflect two groups of REE in the whole-rock compositions. One group includes Lu, Tm, Ho, and Tb with odd atomic numbers at lower, and the other elements Yb, Dy, Gd, Sm, and Y with even atomic numbers at higher, concentrations. Europium and Nd display similar patterns to those of the elements in these groups, whereas La and Ce in zircon and host rocks display a log–log linear positive correlation (Fig. 5B).

The regular pattern and linear positive correlations of trace elements in zircon and host rock (Figs. 5A and B), as well as the related chondrite-normalized zircon REE patterns (Fig. 3E) and zircon compositional fields (Fig. 4) indicate that trace element concentrations in zircon depend on the chemical compositions of their host rocks. However, for HREE and Y in N-MORB-type host rocks this conclusion cannot be made uniformly for all elements, as noted from the "kinks" in the lines connecting bulk rock and zircon data (Figs. 5A and B). This observation encourages the calculation of mineral/whole-rock partition coefficients (labelled as *D* values) for a further evaluation of these system-

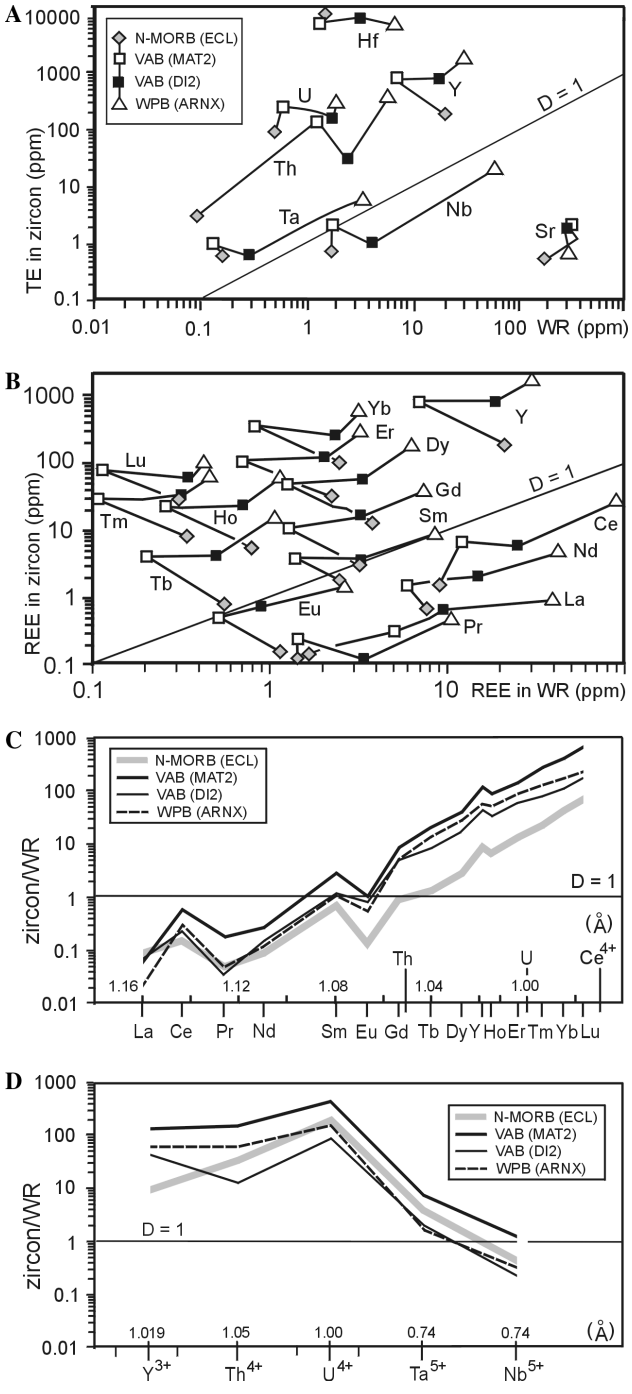

Fig. 5. (A) Whole-rock (WR) versus zircon trace element (TE) concentrations; zircon is given by mean values from analyses in Table 2 and Fig. 4; symbols refer to rock suites in Figs. 2 and 5. Lines correlate zircon mean values and host rock compositions for the same element. (B) Whole-rock (WR) versus zircon REE concentrations; note regular and systematic pattern for some LREE (La, Ce, Pr, and Nd) and HREE with odd and even atomic numbers. (C and D) Zircon/whole-rock (zircon/WR) values, interpreted as mineral/melt values D for trace and rare earth elements (Table 4); calculated from zircon mean values from analyses in Table 2; labels refer to rock suites. The $^{[8]}REE^{3+}$ and trace element ionic radii (in Å) after Shannon (1976) are scaled in (C) and not to scale in (D).

Table 4
Zircon/host rock (mineral/melt *D* values) calculated from the means of zircon analyses in Table 2 and Fig. 4 and whole-rock data in Table 1

Sample rock	ECL ecl-am N-MORB	MAT2 hbl-gn VAB	DI2 hbl-gn VAB	ARNX am WPB
D-Y	8.65	116.70	44.16	56.80
D-Nb	0.42	1.19	0.22	0.31
D-La	0.05	0.06	0.06	0.02
D-Ce	0.15	0.54	0.22	0.27
D-Pr	0.04	0.17	0.03	0.04
D-Nd	0.08	0.25	0.13	0.11
D-Sm	0.70	2.63	0.87	0.96
D-Eu	0.13	0.99	0.80	0.51
D-Gd	0.78	8.09	4.63	4.86
D-Tb	1.37	19.40	8.11	13.67
D-Dy	2.73	37.72	16.52	27.05
D-Ho	6.76	86.01	32.91	49.05
D-Er	12.85	141.63	58.88	84.51
D-Tm	20.66	272.38	78.12	127.72
D-Yb	41.44	400.18	110.82	162.47
D-Lu	72.45	646.31	167.60	221.09
D-Hf	5665	6034	2915	1073
D-Ta	4.07	6.92	1.93	1.60
D-Th	32.97	147.84	12.04	60.45
D-U	184.05	441.40	88.67	149.40

Label of samples as in Table 2.

atics (Tables 1, 2, and 4). For zircon, estimates of such partition coefficients have been made in experimental (Watson, 1980, 1996), analytical (Sano et al., 2002; Thomas et al., 2002) and theoretical approaches (Hinton and Upton, 1991; Guo et al., 1996). Partition coefficients (*D* values) may be used to back-calculate melt compositions and to model magmatic fractionation processes (e.g., Rollinson, 1993). This is problematic in the case of zircon, as zircon/melt *D* values could vary with melt composition (Hoskin and Schaltegger, 2003). Furthermore, the *D* values from felsic igneous rocks are seriously compromised by abundant zircon inherited from magmatic sources. In contrast to zircon in granitic systems (Watson and Harrison, 1983; Hanchar and Watson, 2003), little is known about zircon saturation and dissolution in mafic melts.

The *D* values for LREE in all zircon populations are calculated to <1, but are affected by errors due to low concentrations (Fig. 5C). The *D* values are >1 for the HREE with an ionic radius smaller than Gd (Gd to Lu). Systematically lower *D* values, lower by an order of magnitude, were calculated for the HREE in the N-MORB-type sample, the pattern of which mirrors the patterns for the other rocks. The *D* values for Y are 50–120 for the VAB- and WPB-type samples and 10 for the N-MORB-type sample. This is markedly above the range of values for adjacent HREE with smaller and larger ionic radii (Fig. 5C) and could be an effect of the elevated Y bulk rock abundances of these samples (Fig. 5B).

The *D* values for Th and U are variable at 12–150 and 90–440, respectively, and the values for U^{4+} match those of trivalent cations with equivalent ionic radii (range of values: Figs. 5C and D). Zircon Nb and Ta abundances reflect the bulk rock compositions—but for Nb the *D* values are 0.2–1.2 and for Ta they are 1.5–6.9. As $^{[8]}Nb^{5+}$ and $^{[8]}Ta^{5+}$ have small ionic radii (0.740 Å, Shannon, 1976) compared to tri- and tetravalent cations, the substitution appears to be limited by the charge. Due to similar ionic radii for Nb^{5+} and Ta^{5+}, the difference of their *D* values and the slight preference for Ta substitution could be a function of distortion in the octahedral site of the crystal lattice.

The similarity of the *D* values for the various zircon populations supports a close correlation between trace element abundances in zircon and their host rocks, which indicates that zircon crystallized from a melt, the composition of which composition is represented by the actual host rock. Systematically lower *D* values for HREE and Y in the N-MORB-type sample could be attributed to the physical conditions of crystallization, such as temperature, pressure, and fugacities which might have selectively inhibited substitution.

9. Ce and Eu anomalies in Zircon

A positive Ce anomaly has been recognized as an important feature of chondrite-normalized REE patterns for igneous zircon (Hoskin and Schaltegger, 2003). When Ce^{3+} (ionic radius 1.143 Å) is oxidized to Ce^{4+} (0.970 Å), it behaves like Zr or Hf and is preferably substituted for these elements in comparison to the other LREE. Consequently, a positive Ce anomaly is probably at least partially controlled by the oxygen fugacity of the parental magma, from which zircon crystallized (Hoskin and Schaltegger, 2003). In the REE patterns of the metabasite zircon populations studied here, positive Ce anomalies are significant (Fig. 3E). This is confirmed by the La, Ce, and Pr concentrations in the whole-rock vs zircon diagram (Fig. 5B). The zircon Ce concentrations are coupled to those of the HREE and Y (Fig. 4B). This indicates that a constant fraction of zircon Ce is tetravalent. In contrast, in altered zircon from eclogitic amphibolites, a flat LREE pattern without a distinct Ce anomaly is observed (Fig. 3D). Possibly, there was no more tetravalent Ce present in such zircon.

Metabasite zircon, including the altered crystals, displays a negative Eu anomaly, which is another important characteristic of terrestrial igneous zircon and occurs in combination with a positive Ce anomaly (Hoskin and Ireland, 2000; Belousova et al., 2002; Hoskin and Schaltegger, 2003). The large Eu^{2+} (ionic radius 1.25 Å) is not accommodated easily in the zircon lattice in comparison to Eu^{3+} (1.066 Å), and therefore the magnitude of the negative Eu anomaly should depend on the Eu^{2+}/Eu^{3+} ratio, i.e., the oxidation state during crystallization (Bingen et al., 2004). However, when oxidizing conditions during zircon crystallization prevail, as is indicated by a positive Ce anomaly, most Eu should be trivalent and the large Eu^{2+} ion should not be abundant. Thus, the observed negative Eu anomaly due to the relative incompatibility of the large Eu^{2+} ion should not be expected in these cases and

must be considered a paradox. It may be explained by relative depletion of Eu^{2+} in the melt through selective substitution for Ca in plagioclase (Hoskin et al., 2000; Hoskin and Schaltegger, 2003; Bingen et al., 2004), or in the bulk rock as a whole (Schaltegger et al., 1999). However, the metabasites (host rocks) have no negative Eu anomalies (Fig. 2B) and plagioclase does not appear as a phase that has preferentially substituted Eu^{2+}. Consequently, arguments involving bulk rock Eu^{2+}/Eu^{3+} ratios, Eu^{2+} abundance or crystallization of other phases than zircon cannot be taken into account in the present study. In accordance to data from metabasite zircon populations, Belousova et al. (2002) reported that the size of the negative Eu anomaly (Eu/Eu*) shows a general positive correlation with Y (1.019 Å). Rubatto (2002) stated that the Eu/Eu* value is lower or reduced in metamorphic zircon, with Th/U <0.01. It has to be considered that $^{[8]}Eu^{3+}$ (1.066 Å) competes with $^{[8]}Th^{4+}$ (1.05 Å) in the zircon lattice.

In the metabasite zircon, the Eu as well as Gd values increase whereas the Eu/Eu* ($=Eu/\sqrt{[La * Pr]}$) ratios decrease with increasing Th. This is supported by the observation that the negative Eu anomaly is best developed in zircon from host rocks rich in Th, as is the case in the WPB-type sample ARNX, or in U- and Th-rich zircon from granitoids (Belousova et al., 2002). Therefore, an alternative explanation for the negative Eu anomaly in terrestrial zircon would be a substitution of Eu^{3+} by Th^{4+} with a smaller ionic radius. The Th^{4+} abundance is correlated with that of Gd^{3+} (Fig. 4C). This provides a further argument that Th^{4+} can enter the zircon crystal lattice like the trivalent cations.

10. Th/U ratios in igneous zircon

The crystallization of zircon and recrystallization of protolith zircon during metamorphism at upper amphibolite-facies and higher grades have been widely discussed (Roberts and Finger, 1997; Liati and Gebauer, 1999; Hoskin and Black, 2000; Rubatto, 2002; Bingen et al., 2004). When the trace element patterns are reviewed, the Th/U ratio appears as a criterion to distinguish igneous and metamorphic/recrystallized zircon (Hoskin and Schaltegger, 2003). Both U^{4+} and Th^{4+} substitute for Zr^{4+}, but Th^{4+} is less compatible in the zircon lattice on account of its larger radius. Preferred expulsion of Th^{4+} resulting in decreasing Th/U ratios would be expected as recrystallization of zircon proceeds. This may explain Th/U ratios of <0.1 in igneous zircon that recrystallized during a metamorphic event (Rubatto and Gebauer, 2000; Hoskin and Black, 2000; Rubatto, 2002; Hoskin and Schaltegger, 2003). In metabasite zircon, Th/U ratios are 0.9–1.6 in the WPB-type sample, 0.2–0.9 in the VAB-type rocks, and 0.03 in the N-MORB-type eclogitic amphibolite (Fig. 4H, Table 2). Thus, in some populations Th/U is below the lower limit of 0.3–0.4 for igneous zircon (Schaltegger et al., 1999; Hoskin and Schaltegger, 2003). However, Th/U <0.07 classifies a granulite- and eclogite-facies metamorphic and/or recrystallized zircon (Rubatto, 2002; Bingen et al., 2004). Low Th/U zircon occurs in sample ECL with a high-pressure mineral assemblage including garnet and omphacite but also in sample DI2 that is characterized by a common amphibolite-facies assemblage. It is debatable whether these low Th/U of zircon could be a consequence of either metamorphic recrystallization or represent a primary igneous signature.

Zircon from VAB- and N-MORB-type rocks displays CL internal oscillatory and sector zoning and no recrystallization rims have been found. Thus despite low Th/U values, typical features of igneous zircon prevail. However, the criterion of oscillatory and sector zoning (Corfu et al., 2003) may not be sufficient to exclude metamorphic recrystallization, as Rubatto et al. (1998) suggested that zircon with low Th/U and sector zoning in eclogites crystallized under subsolidus conditions, possibly in the presence of fluids. U–Pb dating of such zircon should show that recrystallized igneous zircon gives progressively younger ages with decreasing Th/U ratios. The N-MORB-type low Th/U zircon population uniformly yielded Pb–Pb single zircon evaporation ages around 590 Ma, which clearly predate the zircon ages from the other metabasites and the well-known regional Variscan and Alpine metamorphic events of 340–260 Ma and 100–30 Ma (Schulz et al., 2004). It can be concluded that zircon in sample ECL has not been affected by younger metamorphic or magmatic events.

A continuous range of Th/U from high "igneous" towards lower "metamorphic" values has been reported from distinct overgrowths on zircon in leucocratic gneisses (Teipel et al., 2004). On the other hand it has been shown that metamorphic zircon may keep the Th/U systematics of its inherited magmatic population during high-grade granulite conditions and that metamorphic zircon of the same age population can have widely different trace element characteristics (Möller et al., 2002, 2003). In such metamorphic zircon, Y and Th/U ratios are not correlated, which suggests that tetravalent and trivalent cations, and thus age, are decoupled (Möller et al., 2003). In metabasite zircon, the homogeneity of Th/U values and their good correlation with Y abundances (Fig. 4G) indicates that coupling was maintained. Rubatto (2002) reported that metamorphic zircon from eclogite has a negligible negative Eu anomaly and lacks the typical HREE enrichment of igneous zircon. In contrast, metabasite zircon with low Th/U displays similar HREE patterns and enrichment as zircon of the other VAB- and WPB-type rocks (Fig. 3E). Low Th/U in metabasite zircon coincides with low Th/U in the host rocks, with Th/U_{WR} of 0.35 in sample ECL compared to Th/U_{WR} of 3.1 in the WPB-type host rock (Fig. 4H). Thus, zircon Th/U depends on and increases with bulk rock Th/U. The coincidence of oscillatory zoning, low Th/U in host rocks, and homogeneously low Th/U correlating with low Y and HREE in zircon suggests equilibration between host rock and zircon at the time of its crystallization. Low

Th/U ratios in zircon from N-MORB-type and some VAB-type host rocks are thus interpreted as a primary igneous feature, and consequently, the Pb–Pb evaporation ages should reflect the crystallization from a melt during a magmatic event.

11. Conclusions

The "xenotime" substitution $(Y, REE)^{3+} + P^{5+} = Zr^{4+} + Si^{4+}$ is the dominant mechanism for trace element substitution in zircon (Speer, 1982; Hanchar et al., 2001; Hoskin and Schaltegger, 2003). With decreasing ionic radii from La^{3+} to Lu^{3+}, the substitution into the zircon lattice becomes progressively easier and thus HREE are enriched in igneous zircon with respect to the LREE (Maas et al., 1992; Hoskin et al., 2000). Hoskin and Schaltegger (2003) claimed that normalized REE patterns show little variation between zircon from different source rocks. However, patterns for these metabasite zircon populations correlated to bulk rock concentrations, display increasing HREE and Y abundances coupled with a decreasing degree of fractionation—with $(Yb/Dy)_N$ decreasing from 20 to 4 (Fig. 3E). Although a close correlation exists, zircon HREE and Y concentrations are not controlled by host rock element abundances alone, as N-MORB-type rocks have lower zircon/host rock partition coefficients for these elements (Figs. 5B and C). Both Nb and Ta correlate with Y and HREE in zircon, indicating that coupled exchanges such as $(Y, REE)^{3+} + (Nb, Ta)^{5+} = 2\ Zr^{4+}$ and $(REE, Fe)^{3+} + (Nb, Ta)^{5+} = 2\ Zr^{4+}$ are operating. A slight preference for Ta over Nb substitution in zircon may be attributed to effects of distortion in octahedral sites. The correlation of Th and U to Y and HREE suggests that substitution of Th^{4+} and U^{4+} is coupled with the xenotime-type exchange. Preference of Th^{4+} with its smaller ionic radius over $Eu^{3+/2+}$ could explain the paradox of a negative Eu anomaly in the presence of a positive Ce anomaly in terrestrial zircon. Low Th/U correlated to low Y and HREE in zircon from low bulk Th/U host rocks appears to be a primary igneous feature that should not be attributed to metamorphic recrystallization (Fig. 4H).

In metabasites, zircon Y and HREE provide the best parameters for discrimination of magmatic provenance. Belousova et al. (2002) considered zircon Hf, apart from Y, as critical for a classification, as Hf in zircon increases with magmatic differentiation (Hoskin and Schaltegger, 2003). In Austroalpine metabasite zircon, Hf abundances are constant for all rock suites and thus unsuitable for discrimination, but they may be used to distinguish zircon from mafic and evolved felsic host rocks, as proposed by Belousova et al. (2002). The normalized REE patterns with positive Ce and negative Eu anomalies, together with HREE enrichment increasing with atomic number and constant Th/U in the metabasite zircon populations allow us to identify zircon that underwent alteration or has submicroscopic mineral inclusions due to deviations from the regular patterns.

Trace element correlations in zircon, together with similar zircon/host rock *D* values, provide arguments that the zircon crystallized from a melt, the composition of which is represented by the composition of the actual host rock. A xenocrystic origin of the zircon can be excluded. The correlated zircon and host rock trace element signatures ensure that igneous signatures can remain preserved through metamorphism and time, which is a pre-condition for the identification of ancient source rocks of detrital zircon. This approach is hampered by the monotony of the REE abundances and patterns in zircon from a wide range of common crustal rocks (Heaman et al., 1990; Hoskin and Ireland, 2000; Hoskin and Schaltegger, 2003). The finding that host rock related trace element variations in metabasite zircon remain preserved will be of limited use in sedimentary provenance studies, as zircon is very rare in mafic rocks and sediments will be dominated by zircon from felsic igneous rocks. However, zircon allows the radiometric dating of mafic rocks. Therefore, its trace element characteristics provide valuable information on igneous crystallization as well as criteria for the geological interpretation of the radiometric data in terms of magmatic protoliths and sources, metamorphism, and metasomatism.

Acknowledgments

Detailed and constructive reviews by F. Corfu, E.A. Belousova, and M. Bröcker are gratefully acknowledged. The language of the manuscript has been improved by J. Craddock, Macalester College, St. Paul, MN, USA. Furthermore, we thank W.U. Reimold for his editorial handling. The LA-ICP-MS analyses at Institut für Mineralogie und Kristallstrukturlehre, University of Würzburg, Germany, were funded through the Deutsche Forschungsgemeinschaft (Project SCHU 676/8).

Associate editor: W. Uwe Reimold

References

Belousova, E.A., Griffin, W.L., O'Reilly, S.Y., Fisher, N.I., 2002. Igneous zircon: trace element composition as an indicator of source rock type. *Contrib. Mineral. Petrol.* **143**, 602–622.

Bingen, B., Austrheim, H., Whitehouse, M.J., Davis, W.J., 2004. Trace element signature and U–Pb geochronology of eclogite-facies zircon, Bergen Arcs, Caledonides of W Norway. *Contrib. Mineral. Petrol.* **147**, 671–683.

Bodet, F., Schärer, U., 2000. Evolution of the SE-Asian continent from U–Pb and Hf isotopes in single grains of zircon and baddeleyite from large rivers. *Geochim. Cosmochim. Acta* **64**, 2067–2091.

Brätz, H., Klemd, R., 2002. Analysis of rare earth elements in geological samples by Laser Ablation-Inductively Coupled Plasma Mass Spectrometry (LA-ICP-MS). Online publication: No. 5988-6305EN, Agilent Technologies.

Chesner, C.A., 1998. Petrogenesis of the Toba Tuffs, Sumatra, Indonesia. *J. Petrol.* **39**, 397–438.

Connelly, J.N., 2000. Degree of preservation of igneous zonation in zircon as a signpost for concordancy in U/Pb geochronology. *Chem. Geol.* **172**, 25–39.

Corfu, F., Hanchar, J.M., Hoskin, P.W.O., Kinny, P., 2003. Atlas of zircon textures. In: Hanchar, J.M., Hoskin, P.W.O. (Eds.), *Zircon. Rev. Mineral. Geochem.*, vol. 53. The Mineralogical Society of America, Washington, pp. 469–500.

Govindaraju, K., 1994. Compilation of working values and sample description for 383 Geostandards. *Geostand. Newsl. Spec. Issue*, vol. 18, pp. 1–158.

Guo, J., Reilly, S.Y., Griffin, W.L., 1996. Zircon inclusions in corundum megacrysts: I. Trace element geochemistry and clues to the origin of corundum megacrysts in alkali basalts. *Geochim. Cosmochim. Acta* **60**, 2347–2363.

Hanchar, J.M., Finch, R.J., Hoskin, P.W.O., Watson, E.B., Cherniak, D.J., Mariano, A.N., 2001. Rare earth elements in synthetic zircon: part I. Synthesis, and rare earth element and phosphorous doping. *Am. Mineral.* **86**, 667–680.

Hanchar, J.M., Miller, C.F., 1993. Zircon zonation patterns as revealed by cathodoluminescence and backscattered electron images: implications for interpretation of complex crustal histories. *Chem. Geol.* **110**, 1–13.

Hanchar, J.M., Watson, B.E., 2003. Zircon saturation thermometry. In: Hanchar, J.M., Hoskin, P.W.O. (Eds.), *Zircon. Rev. Mineral. Geochem.*, vol. 53. The Mineralogical Society of America, Washington, pp. 89–112.

Heaman, L.M., Bowsin, R., Crocket, J., 1990. The chemical compositions of igneous zircon suites: implications for geochemical tracer studies. *Geochim. Cosmochim. Acta* **54**, 1597–1607.

Hinton, R.W., Upton, B.G.J., 1991. The chemistry of zircon: variations within and between large crystals from syenite and alkali basalt xenoliths. *Geochim. Cosmochim. Acta* **55**, 3287–3302.

Hoinkes, G., Koller, F., Rantitsch, G., Dachs, E., Höck, V., Neubauer, F., Schuster, R., 1999. Alpine metamorphism of the Eastern Alps. *Swiss Bull. Mineral. Petrol.* **79**, 155–181.

Horn, I., Hinton, R.W., Jackson, S.E., Longerich, H.P., 1997. Ultra-trace element analysis of NIST SRM 616 and 614 using laser ablation microprobe-inductively coupled plasma-mass spectrometry (LAM-ICP-MS): a comparison with secondary ion mass spectrometry (SIMS). *Geostand. Newslett.* **21**, 191–203.

Hoskin, P.W.O., Black, L.P., 2000. Metamorphic zircon formation by solid-state recrystallization of protolith igneous zircon. *J. Metamorph. Geol.* **18**, 423–439.

Hoskin, P.W.O., Ireland, T.R., 2000. Rare earth element chemistry of zircon and its use as a provenance indicator. *Geology* **28**, 627–630.

Hoskin, P.W.O., Kinny, P.D., Wyborn, D., Chappell, B.W., 2000. Identifying accessory mineral saturation during differentiation in granitoid magmas: an integrated approach. *J. Petrol.* **41**, 1365–1396.

Hoskin, P.W.O., Schaltegger, U., 2003. The composition of zircon and igneous and metamorphic petrogenesis. In: Hanchar, J.M., Hoskin, P.W.O. (Eds.), *Zircon. Rev. Mineral. Geochem.*, vol. 53. The Mineralogical Society of America, Washington, pp. 27–62.

Jackson, S.E., Longerich, H.P., Dunning, G.R., Fryer, B.J., 1992. The application of laser ablation microprobe-inductively coupled plasma-mass spectrometry (LAM-ICP-MS) to in situ trace element determination in minerals. *Can. Mineral.* **30**, 1049–1064.

Jain, J.C., Neal, C.R., Hanchar, J.M., 2001. Problems associated with the determination of rare earth elements of a "gem" quality zircon by inductively coupled plasma-mass spectrometry. *Geostand. Newslett. J. Geostand. Geoanal.* **25**, 229–237.

Liati, A., Gebauer, D., 1999. Constraining the prograde and retrograde P–T–t path of Eocene HP rocks by SHRIMP dating of different zircon domains: inferred rates of heating, burial, cooling and exhumation for central Rhodope, northern Greece. *Contrib. Mineral. Petrol.* **125**, 340–354.

Maas, R., Kinny, P.D., Williams, I.S., Froude, D.O., Compston, W., 1992. The Earth's oldest known crust: a geochronological and geochemical study of 3900–4200 Ma old detrital zircon from Mt. Narryer and Jack Hill, Western Australia. *Geochim. Cosmochim. Acta* **56**, 1281–1300.

McDonough, W.F., Sun, S.S., 1995. The composition of the earth. *Chem. Geol.* **120**, 223–253.

Möller, A., O'Brien, P.J., Kennedy, A., Kröner, A., 2002. Polyphase zircon in ultrahigh-temperature granulites (Rogaland, SW Norway): constraints for Pb diffusion in zircon. *J. Metamorph. Geol.* **20**, 727–740.

Möller, A., O'Brien, P.J., Kennedy, A., Kröner, A., 2003. Linking growth episodes of zircon and metamorphic textures to zircon chemistry: an example from the ultrahigh-temperature granulites of Rogaland (SW Norway). In: Vance, D., Villa, I., Müller, W. (Eds.), *Geochronology: Linking the Isotopic Record with Petrology and Textures. Geol. Soc. London Spec. Publ.*, vol. 220. The Geological Society of London, pp. 65–81.

Murali, A.V., Parthasarathy, R., Mahadevan, T.M., Sankar Das, M., 1983. Trace element characteristics, REE patterns and partition coefficients of zircons from different geological environments—a case study on Indian zircons. *Geochim. Cosmochim. Acta* **47**, 2047–2052.

Norman, M.D., Pearson, N.J., Sharma, A., Griffin, W.L., 1996. Quantitative analysis of trace elements in geological materials by laser ablation ICPMS: instrumental operating conditions and calibration values of NIST glasses. *Geostand. Newslett.* **20**, 247–261.

Pearce, J.A., 1982. Trace element characteristics of lavas from destructive plate boundaries. In: Thorpe, R.S. (Ed.), *Andesites*. Wiley, Chichester, pp. 525–548.

Pearce, N.J.G., Perkins, W.T., Westgate, J.A., Gorton, M.P., Jackson, S.E., Neal, C.R., Chenery, S.P., 1997. A compilation of new and published major and trace element data for NIST SRM 610 and NIST SRM 612 glass reference materials. *Geostand. Newslett.* **21**, 115–144.

Roberts, M.P., Finger, F., 1997. Do U–Pb zircon ages from granulites reflect peak metamorphic conditions?. *Geology* **25** 319–322.

Rollinson, H.R., 1993. *Using Geochemical Data: Evaluation, Presentation, Interpretation*. Longman Scientific and Technical, London, pp. 1–352.

Rubatto, D., 2002. Zircon trace element geochemistry: partitioning with garnet and the link between U–Pb ages and metamorphism. *Chem. Geol.* **184**, 123–138.

Rubatto, D., Gebauer, D., 2000. Use of cathodoluminescence for U–Pb zircon dating by ion microprobe: some examples from the Western Alps. In: Pagel, M., Barbin, V., Blanc, P., Ohnenstetter, D. (Eds.), *Cathodoluminescence in Geosciences*. Springer, Berlin, Heidelberg, New York, pp. 373–400.

Rubatto, D., Gebauer, D., Fanning, M., 1998. Jurassic formation and Eocene subduction of the Zermatt—Saas-Fee ophiolites: implications for the geodynamic evolution of the Central and Western Alps. *Contrib. Mineral. Petrol.* **132**, 269–287.

Rupasinghe, M.S., Dissanayake, C.B., 1987. The geochemistry and mineralogy of zircons from Sri Lanka. *Bull. Geol. Soc. Finland* **59**, 3–19.

Sano, Y., Terada, K., Fukoka, T., 2002. High mass resolution ion microprobe analysis of rare earth elements in silicate glass, apatite and zircon: lack of matrix dependency. *Chem. Geol.* **184**, 217–230.

Schaltegger, U., Fanning, C.M., Günther, D., Maurin, J.C., Schulmann, K., Gebauer, D., 1999. Growth, annealing and recrystallization of zircon and preservation of monazite in high-grade metamorphism: conventional and in-situ U–Pb isotope, cathodoluminescence and microchemical evidence. *Contrib. Mineral. Petrol.* **134**, 186–201.

Schönhofer, R., 1999. Das ostalpine Altkristallin der westlichen Lasörlinggruppe (Osttirol, Österreich): Kartierung, Stoffbestand und tektonometamorphe Entwicklung. *Erlanger geologische Abhandlungen* **130**, 1–128, Lehrstuhl für Geologie, Universität Erlangen-Nürnberg (in German with English Abstr.).

Schulz, B., 1990. Prograde-retrograde P–T–t-deformation path of Austroalpine micaschists during Variscan continental collision (Eastern Alps). *J. Metamorph. Geol.* **8**, 629–643.

Schulz, B., 1993. Mineral chemistry, geothermobarometry and pre-Alpine high-pressure metamorphism of eclogitic amphibolites and mica schists from the Schobergruppe, Austroalpine basement, Eastern Alps. *Mineral. Mag.* **57**, 189–202.

Schulz, B., 1995. Geochemistry and REE magmatic fractionation patterns in the Prijakt amphibolitized eclogites of the Schobergruppe, Austroalpine basement (Eastern Alps). *Swiss Bull. Mineral. Petrol.* **75**, 225–239.

Schulz, B., 1997. Pre-Alpine tectonometamorphic evolution in the Austroalpine basement to the south of the central Tauern Window. *Swiss Bull. Mineral. Petrol.* **77**, 281–297.

Schulz, B., Bombach, K., 2003. Single zircon Pb–Pb geochronology of the Early-Palaeozoic magmatic evolution in the Austroalpine basement to the south of the Tauern Window. *J. Geol. Bundesanstalt* **143**, 303–321.

Schulz, B., Nollau, G., Heinisch, H., Godizart, G., 1993. Austro-Alpine basement complex to the south of the Tauern Window. In: von Raumer, J., Neubauer, F. (Eds.), *The Pre-Mesozoic Geology in the Alps*. Springer, Berlin, Heidelberg, New York, pp. 493–512.

Schulz, B., Bombach, K., Pawlig, S., Brätz, H., 2004. Neoproterozoic to Early-Palaeozoic magmatic evolution in the Gondwana-derived Austroalpine basement to the south of the Tauern Window (Eastern Alps). *Int. J. Earth Sci.* **93**, 824–843..

Shannon, R.D., 1976. Revised effective ionic radii and systematic studies of interatomic distances in halides and chalcogenides. *Acta Crystallogr. Sect. A* **32**, 751–767.

Shannon, W.M., Barnes, C.G., Bickford, M.E., 1997. Grenville magmatism in West Texas: petrology and geochemistry of the Red Bluff Granitic Suite. *J. Petrol.* **38**, 1279–1305.

Snyder, G.A., Taylor, L.A., Crozaz, G., 1993. Rare earth element selenochemistry of immiscible liquids and zircon at Apollo 14: an ion probe study of evolved rocks on the moon. *Geochim. Cosmochim. Acta* **57**, 1143–1149.

Speer, J.A., 1982. *Zircon. Reviews in Mineralogy 5*, second ed. Mineralogical Society of America, Washington, pp. 67–112.

Sylvester, P.J., 2003. Trace element analysis of fused whole rock glasses by laser ablation ICPMS. In: Sylvester, P.J. (Ed.), *Laser-Ablation ICPMS in the Earth Sciences. Principles and Applications. Mineralogical Association of Canada Short Course Series*, vol. 29. Mineralogical Association of Canada, Toronto, pp. 147–162.

Teipel, U., Eichhorn, R., Loth, G., Rohrmüller, J., Höll, R., Kennedy, A., 2004. U–Pb SHRIMP and Nd isotopic data from the western Bohemian Massif (Bayerischer Wald, Germany): implications for Upper Vendian and Lower Ordovician magmatism. *Int. J. Earth Sci.* **93**, 782–801.

Thomas, J.B., Bodnar, R.J., Shimizu, N., Sinha, A.K., 2002. Determination of zircon/melt trace element partition coefficients from SIMS analysis of melt inclusions in zircon. *Geochim. Cosmochim. Acta* **66**, 2887–2901.

Vavra, G., 1994. Systematics of internal zircon morphology in major Variscan granitoid types. *Contrib. Mineral. Petrol.* **117**, 331–344.

Von Raumer, J.F., Neubauer, F., 1993. Late Precambrian and Palaeozoic evolution of the Alpine basement—an overview. In: von Raumer, J., Neubauer, F. (Eds.), *The Pre-Mesozoic Geology in the Alps*. Springer, Berlin, Heidelberg, New York, pp. 625–639.

Von Raumer, J.F., Stampfli, G.M., Bussy, F., 2003. Gondwana-derived microcontinents—the constituents of the Variscan and Alpine collisional orogens. *Tectonophysics* **365**, 7–22.

Watson, B.E., 1980. Some experimentally determined zircon/liquid partition coefficients for the rare earth elements. *Geochim. Cosmochim. Acta* **44**, 895–897.

Watson, B.E., 1996. Surface enrichment and trace-element uptake during crystal growth. *Geochim. Cosmochim. Acta* **60**, 5013–5020.

Watson, B.E., Harrison, T.M., 1983. Zircon saturation revisited: temperature and composition effects in a variety of crustal magma types. *Earth Planet. Sci. Lett.* **64**, 295–304.

Wilde, S.A., Valley, J.W., Peck, W.H., Graham, C.M., 2001. Evidence from detrital zircons for the existence of continental crust and oceans on the Earth 4.4 Gyr ago. *Nature* **409**, 175–178.

Wilson, M., 1989. *Igneous Petrogenesis. A Global Tectonic Approach*. Chapman and Hall, London, 446 pp.